Activation of Methane by the Iron Dimer Cation. A Theoretical Study

Sandro Chiodo, Ivan Rivalta, Maria del Carmen Michelini, Nino Russo, and Emilia Sicilia*

Dipartimento di Chimica and Centro di Calcolo ad Alte Prestazioni per Elaborazioni Parallele e Distribuite-Centro d'Eccellenza MURST, Università della Calabria, I-87030 Arcavacata di Rende, Italy

Jesus M. Ugalde

Kimika Fakultatea, Euskal Herriko Unibertsitatea, P.K. 1072, 20080 Donostia, Euskadi, Spain

Received: July 20, 2006; In Final Form: September 12, 2006

A detailed investigation of the reaction mechanisms underlying the observed reactivity of the iron dimer cation with respect to methane has been performed by density functional hybrid (B3LYP) and nonhybrid (BPW91) calculations. Minima and transition states have been fully optimized and characterized along the potential energy surfaces leading to three different exit channels for both the ground and the first excited states of the dimer. A comparison with our previous work covering the reactivity of the Fe^+ monomer was made to underline similarities and differences of the reaction mechanisms. Results show that geometric arrangements corresponding to bridged positions of the ligands with respect to iron atoms are always favored and stabilize intermediates, transition states and products, facilitating their formation. Binding energies of reaction products have been computed and compared with experimental measurements, and ELF analysis of the bond has been performed to rationalize trends as a function of the structure.

Introduction

Methane activation by transition metals has been a topic of growing interest during the past two decades, due to economic interest in methane conversion and chemistry. Significant insights into the details and mechanisms of the activation process can be gained by studies of gas-phase reactions of metal ions. The application of mass spectrometry, guided ion beam techniques, and theoretical studies have been important in clarifying mechanistic aspects, developing metal−ligand bond energy data, and comprehensively exploring the intrinsic properties of transition-metal chemistry.[1−21] However, bare metal cations are oversimplified models with respect to real catalysts involved in processes occurring on bulk phase surfaces. Clusters may better serve to this aim because they lie between the atomic scale and that of the solid state so that they are ideally suited to serve as a probe for the transition between these two forms of matter. Moreover, they are sufficiently simple to be successfully modeled by theoretical high-level calculations. For instance, the recent characterization[22] of the intermediates structures for the CO dissociation on transition metal surfaces has been achieved by a detailed investigation of the $Sc_2\eta^2$-(μ_2-C,O) dinuclear scandium−carbonyl species, thus highlighting the interest in studying the chemistry of small clusters.

Although more extensive work is required to prove how good the analogy between clusters and surfaces might be, metal clusters represent simplified systems where elementary reactions can be studied in microscopic detail, as a function of cluster composition, size and charge. In this perspective, bond activation of small hydrocarbons by a variety of metal clusters became the subject of several experimental works,[23−30] the attention being mainly focused on the large variation of reactivity with the cluster size.

In the case of iron, it is considered to be a good catalyst for the C−H bond activation of methane, able to significantly reduce the C−H bond activation energy. However, little fundamental work exists in the literature concerning this process occurring on iron surfaces.[31] The behavior of iron clusters with respect to small hydrocarbons was examined by Irion and co-workers.[25a,b] More recently, the interest in these clusters was renewed by a work by Armentrout et al.[28] on the methane activation by size-selected iron cluster cations, Fe_n^+ ($n = 2-15$), performed using guided ion beam mass spectrometry. The main reactions observed are dehydrogenation, double dehydrogenation and elimination of CH_3 to form $Fe_nCH_2^+$, Fe_nC^+ and FeH^+, respectively. Results of the analysis of energy dependence prove the existence of barriers in excess of the endothermicity, except for $n = 3$ and 4, for the initial hydrogen elimination process. As repeatedly outlined,[28] however, definitive conclusions concerning the trends and the reaction mechanisms cannot be made without complementary theoretical information on the structures of the involved species. To complement the experimental observations, density functional theory (DFT), which includes electronic correlation at a lower computational cost than traditional molecular orbital ab initio methods, is a logical alternative to undertaking theoretical investigations of systems that require a large number of calculations, as in the present case.

The electronic structure of iron clusters was the subject of a number of theoretical studies at several levels of theory,[32−47] including an investigation carried out by us at the density functional level for the dimer. Limited is the number, on the contrary, of the works that deal with a detailed theoretical analysis of the interaction and activation of small molecules by the same clusters.[48−52] Such an analysis, in particular, was not performed until now for the activation of methane. Our previous work on the insertion of bare metal cations into the bonds of prototypical molecules already covers the theoretical study of

* Address correspondence to this author. Tel. +39-0984-492048. Fax: +39-0984-492044. E-mail: siciliae@unical.it.

10.1021/jp064611a CCC: $33.50
Published on Web 10/26/2006

the methane activation by the Fe^+ cation.[18] Therefore, we have chosen to extend this study to CH_4 activation occurring on small iron cationic clusters ($n = 1-4$). In the current paper we report our results for the dimer, which is the smallest of the clusters made and proved experimentally and is the more amenable to be theoretically treated. Hence, it can be considered some kind of benchmark system from which to start the investigation of the reactivity patterns of larger clusters. The reactivity of the trimer and tetramer is actually under investigation. The electronic structure of the dimer is also reexamined in light of the use of a newly developed basis set of double-ζ quality.

Computational Details

Geometry optimizations as well as frequency calculations for all the reactants, intermediates, products and transition states were performed at the density functional level of theory. An intensive work has recently been carried out to test the reliability of the available DF exchange−correlation functionals in reproducing the properties of transition metals containing systems.[53−58] A definitive conclusion, at least about the possibility to choose between *hybrid* and *nonhybrid* DFT, is far from being reached. Therefore, in the present work both Becke's three-parameter hybrid functional[59] combined with the Lee, Yang and Parr (LYP)[60] correlation functional, denoted as B3LYP, and the BPW91 exchange-correlation functional, which is composed of Becke's exchange[61] and Perdew−Wang's correlation,[62] were used. Previous experience of our groups shows that the B3LYP functional associated with the use of the DZVP[63] basis set is a reasonable choice, conjugating accuracy of the results with low computational cost, to treat first-row transition metal containing systems. On the other hand, previous computations performed for bare iron clusters[47] concluded that the performance of the BPW91 functional is superior to that of B3LYP functional for systems containing metal−metal bonds. Moreover, as is already well-known, one of the drawbacks of density functional approaches is the incorrect prediction of the energy ordering of the states of atoms and cations. This just occurs in the case of the Fe^+ cation for which the ground $^6D(3d^6s^1)$ state is put above the $^4F(3d^7)$ excited state. The requirement to obtain a correct reference energy for the ground state of first-row transition metal cations prompted us to introduce new basis sets, which improves the description of the ground and low lying excited states, optimized at both B3LYP and BPW91 levels. More details concerning the optimization procedure that, starting from the traditional DZVP[63] basis sets, optimized for local functionals, gives the new ones can be found elsewhere.[64] The exponents and contraction coefficients for the B3LYP optimized basis set can be found in the same ref 64, and those for the newly optimized basis set for the BPW91functional are reported in Table 1.

At the B3LYP level and with the corresponding optimized DZVP basis set, the correct ground state of the iron cation is predicted. However, with respect to the value of 5.76 kcal/mol of the experimental gap[65] between the ^6D ($4s3d^6$) ground state of the iron cation and the ^4F ($3d^7$) first excited one, an overestimated value of 12.40 kcal/mol is obtained. A more stringent agreement is obtained using the BPW91 functional along with the corresponding optimized basis set as the value of the gap is 3.37 kcal/mol.

Optimized DZVP basis sets for iron, from now on indicated as $DZVP_{opt}$, and the traditional TZVP[66] ones for the other atoms were used to locate minima and transition states relevant for the examined processes and to build up the corresponding potential energy surfaces. For the sake of clarity we will refer to these levels of computation as B3LYP/$DZVP_{opt}$ and BPW91/$DZVP_{opt}$, emphasizing the role of the basis set used for the metal.

TABLE 1: Exponents and Contraction Coefficients Relative to the BPW91 Optimized DZVP Basis Set

subset	exponents	contraction coefficients
s	61430.2300000000	0.0017600000
	9222.1760000000	0.0134100000
	2097.5970000000	0.0666400000
	591.4904000000	0.2280600000
	191.8606000000	0.4680700000
	65.8263200000	0.3602900000
s	128.7407000000	−0.1090400000
	14.7181300000	0.6471100000
	5.9507540000	0.4614800000
s	10.8598800000	−0.2450600000
	1.7194470000	0.7638300000
	0.6664531000	0.3830400000
s	0.9754761000	−0.1722700000
	0.1231143000	0.6612500000
s	0.0448795000	1.0000000000
p	780.6203000000	0.0091100000
	184.0062000000	0.0675800000
	58.0844700000	0.2576400000
	20.7597900000	0.5046000000
	7.5934510000	0.3385300000
p	4.0279170000	0.3515500000
	1.5264700000	0.6108000000
	0.5573702000	0.2413100000
p	0.1210000000	1.0000000000
d	23.9293200000	0.0619000000
	6.3999010000	0.2696100000
	1.9317420000	0.4892400000
	0.5115279000	0.4553300000
d	0.0900000000	1.0000000000

Several initial structures have been optimized for each step of the reaction to take into account different ways of coordination. Because the spin state of the complexes under investigation is experimentally unknown, the optimization of each complex was carried out for several multiplicities and the possible occurrence of spin crossing between surfaces of different multiplicity was examined.[67]

For all the studied species we have checked $\langle S^2 \rangle$ values to assess whether spin contamination can influence the quality of the results. In all cases we have found that the calculated values differ from $S(S + 1)$ by less that 10%.

To locate stationary points on the PES, no symmetry and geometry restrictions were imposed during geometry optimization. Vibrational analysis was performed in the harmonic approximation for each optimized stationary point to determine its character (minimum or saddle point) and to evaluate the zero-point vibrational energy (ZPVE) corrections, which are included in all relative energies, thermal energy corrections and entropy contributions. For transition states it was carefully checked that the vibrational mode associated to the imaginary frequency corresponds to the correct movement of involved atoms.

The counterpoise corrections have been calculated to correct binding energies (BE) for basis set superposition error (BSSE).[68] The introduced corrections for some of the considered complexes change significantly the noncorrected values.

All the calculations reported in the present work have been carried out with the GAUSSIAN98/DFTcode.[69]

A topological description of the electron density of some product fragments has been carried out to characterize the bonding. In particular, we have used the topological analysis of the chemical bond proposed by Silvi and Savin,[70] which relies upon the gradient field analysis of the electron localization function (ELF) of Becke and Edgecombe.[71] ELF calculations

TABLE 2: Electronic State, Valence Electronic Configuration, Bond Length, in Å, Vibrational Frequency, in cm^{-1}, and Relative Energy, in kcal/mol, at the B3LYP/$DZVP_{opt}$ and BPW91/$DZVP_{opt}$ Levels of Theory of a Number of Selected Electronic States of Fe_2^+

		B3LYP			BPW91		
state	configuration	R_e	ω_e	ΔE	R_e	ω_e	ΔE
Σ_u^{10+}	$(3d\sigma_g)^2\,(3d\pi_u)^2\,(3d\delta_g)^2\,(3d\delta_u^*)^2\,(3d\pi_g^*)^2\,(3d\sigma_u^*)^2(4s\sigma_g)^2(4s\sigma_u^*)^1$	2.987	134	0.00	2.953	139	53.6
Σ_g^{10+}	$(3d\sigma_g)^1\,(3d\pi_u)^4\,(3d\delta_g)^2\,(3d\delta_u^*)^2\,(3d\pi_g^*)^2\,(3d\sigma_u^*)^1(4s\sigma_g)^2(4s\sigma_u^*)^1$	2.443	224	15.5	2.399	224	24.2
$^{10}\Delta_g$	$(3d\sigma_g)^2\,(3d\pi_u)^2\,(3d\delta_g)^3\,(3d\delta_u^*)^2\,(3d\pi_g^*)^2\,(3d\sigma_u^*)^1(4s\sigma_g)^2(4s\sigma_u^*)^1$	2.731	174	26.6	2.759	166	46.5
Σ_g^{10-}	$(3d\sigma_g)^1\,(3d\pi_u)^2\,(3d\delta_g)^4\,(3d\delta_u^*)^2\,(3d\pi_g^*)^2\,(3d\sigma_u^*)^1(4s\sigma_g)^2(4s\sigma_u^*)^1$	2.808	168	41.5	2.853	135	44.1
Σ_u^{8+}	$(3d\sigma_g)^2\,(3d\pi_u)^4\,(3d\delta_g)^2\,(3d\delta_u^*)^2\,(3d\pi_g^*)^2\,(3d\sigma_u^*)^1\,(4s\sigma_g)^2$	2.093	382	1.6	2.110	363	1.7
$^8\Delta_u$	$(3d\sigma_g)^1\,(3d\pi_u)^4\,(3d\delta_g)^3\,(3d\delta_u^*)^2\,(3d\pi_g^*)^2\,(3d\sigma_u^*)^1\,(4s\sigma_g)^2$	2.233	313	9.6	2.212	304	0.0
$^8\Delta_g$	$(3d\sigma_g)^1\,(3d\pi_u)^4\,(3d\delta_g)^2\,(3d\delta_u^*)^3\,(3d\pi_g^*)^2\,(3d\sigma_u^*)^1\,(4s\sigma_g)^2$	2.321	293	18.9	2.304	284	8.3
Σ_u^{8-}	$(3d\sigma_g)^2\,(3d\pi_u)^2\,(3d\delta_g)^4\,(3d\delta_u^*)^2\,(3d\pi_g^*)^2\,(3d\sigma_u^*)^1\,(4s\sigma_g)^2$	2.407	256	34.1	2.445	239	27.4
$^6\Delta_u$	$(3d\sigma_g)^1\,(3d\pi_u)^4\,(3d\delta_g)^3\,(3d\delta_u^*)^2\,(3d\pi_g^*)^2\,(3d\sigma_u^*)^1\,(4s\sigma_g)^2$	2.232	308	51.0	2.212	301	35.3
Σ_u^{6+}	$(3d\sigma_g)^1\,(3d\pi_u)^4\,(3d\delta_g)^2\,(3d\delta_u^*)^2\,(3d\pi_g^*)^4\,(3d\sigma_u^*)^1\,(4s\sigma_g)^1$	2.633	199	51.6	2.590	212	66.2
$^6\Delta_g$	$(3d\sigma_g)^2\,(3d\pi_u)^4\,(3d\delta_g)^2\,(3d\delta_u^*)^2\,(3d\pi_g^*)^2\,(4s\sigma_g)^2$	1.924	3484	53.9	1.959	440	25.0
Σ_u^{6-}	$(3d\sigma_g)^1\,(3d\pi_u)^4\,(3d\delta_g)^4\,(3d\delta_u^*)^2\,(3d\pi_g^*)^2\,(3d\sigma_u^*)^1\,(4s\sigma_g)^1$	2.215	312	87.9	2.245	290	59.5

have been carried out with the TopMod package developed at the Laboratoire de Chimie Théorique de l'Université Pierre et Marie Curie.[72,73] Isosurfaces have been visualized with MOLEKEL visualization package.[74]

Results and Discussion

Structure of Iron Dimer. As it was extensively discussed in our previous paper on this subject,[46] the description of the electronic structure of the neutral and charged dimers of the middle first-row transition metals is particularly challenging. This difficulty is usually attributed to the *pseudo* half-filled 3d shells of the constituent atoms and is clearly reflected by the uncertainty of a definitive designation of their ground states. Actual results for energy, bond length and vibrational frequency of a number of selected electronic state of Fe_2^+ obtained employing the newly optimized $DZVP_{opt}$ basis sets for the B3LYP and BPW91 functionals are collected in Table 2. Two levels of theory were employed in our previous work, that is optimization at B3LYP/TZVP+G(3df,2p)[14] and single point calculations at CCSD(T)/TZVP+G(3df,2p)//B3LYP/TZVP+G(3df,2p) levels of theory. Both approaches agree at predicting decaplets, octets and sextets as the most stable states, whereas quartets and doublets states are found to lie more than 4.0 eV higher in energy. However, the CCSD(T)/TZVP+G(3df,2p)//B3LYP/TZVP+G(3df,2p) level of theory suggests that the Σ_g^{10-} state is the most stable one, with the state Σ_u^{8+} lying only 3.2 kcal/mol higher in energy. On the other hand, B3LYP/TZVP+G(3df,2p) predicts the Σ_u^{8+} as the ground state of Fe_2^+ and places the Σ_g^{10-} state 53.0 kcal/mol higher. The closest decaplet state, in this case, is predicted to be the Σ_u^{10+} that lies 16.6 kcal/mol above. In the already cited ref 47 $^8\Delta_u$ is identified as the ground state of the iron dimer cation at the BPW91/6-311+G* level of theory. Sextet $^6\Delta_g$ and $^6\Delta_u$ excited states lie about 29 kcal/mol above and the first decaplet Σ_g^{10-} excited state is predicted to be only by 1.4 kcal/mol less stable than sextet states. Using the DZVP basis sets newly optimized for the B3LYP and BPW91 functionals, the energy ordering of the states changes significantly and the identification of the ground state is not unique. At the hybrid B3LYP level the ground state corresponds to the most stable decaplet Σ_u^{10+} state, separated by only 1.6 kcal/mol from the excited Σ_u^{8+} state. All the sextet states are significantly higher in energy and the most stable sextet, $^6\Delta_u$, is situated 51.10 kcal/mol above the assigned ground state. According to previous BPW91 computations, at this level of theory the $^8\Delta_u$ is identified as the ground state. The closest decaplet excited state is Σ_g^{10+}, whcih is separated by 24.2 kcal/mol from the ground state and more stable by only 0.8 kcal/mol than the lowest sextet $^6\Delta_g$ state.

Activation of Methane C−H Bond by Fe^+. Before discussing the results for the reaction under investigation, we review those previously obtained for the state-specific reaction of iron cation with methane.[21] On the basis of experimental data[75,76] three reaction channels were investigated: dehydrogenation, which is the most thermodynamically favored process, and elimination of H and CH_3 fragments to obtain $FeCH_3^+$ and FeH^+, respectively. Formation of these latter reaction products becomes accessible at higher energies. The proposed mechanism involves formation of an initial ion−molecule complex, $FeCH_4^+$, more stable in a quartet ground state. Due to the change of multiplicity with respect to the reactants, in this region the unique spin crossing between surfaces of different multiplicities occurs, after which the reaction proceeds, conserving the spin. The binding energy of the complex $FeCH_4^+$ with respect to the sextet ground state of the cation is evaluated to be 10.9 kcal/mol, in very good agreement with the measured value of 13.7±0.8 kcal/mol.[77] The first adduct, through the migration of a hydrogen atom from carbon to the metal, yields the insertion intermediate, $H-Fe^+-CH_3$, whose formation is the key step of the whole process. This intermediate is situated at 4.3 kcal/mol above the sextet reactant asymptote, and the transition state to obtain it is only 5.3 kcal/mol higher in energy than the dissociation limit. Formation of the last intermediate along the PES for the hydrogen elimination, $H_2-FeCH_2^+$, requires overcoming a very high energy barrier, in excess of 40.7 kcal/mol with respect to the entrance channel, corresponding to a tight four-center transition state. From the molecular hydrogen complex, by loss of H_2, products are directly formed. The calculated value of the endothermicity of this process is 30 kcal/mol, in excellent agreement with the value of 29.1 ± 1.2 experimentally predicted.[77] A simple bond breaking generates the other two ionic products, $FeCH_3^+$ and FeH^+, directly from the insertion intermediate and with endothermicities of 44.5 and 47.6 kcal/mol, respectively. These values compare fairly well with the experimentally reported ones,[75] that is, 49.8 and 55.6 kcal/mol, respectively. In Figure 1 are sketched the reaction paths for the sextet and quartet states of iron cation.

Activation of Methane C−H Bond by Fe_2^+. Experimental studies[28] of the reactivity of cationic iron dimer toward methane show that, among the reactions that occur without iron atom loss, the dominant process at all energies is the hydride formation:

$$Fe_2^+ + CH_4 \rightarrow Fe_2H^+ + CH_3$$

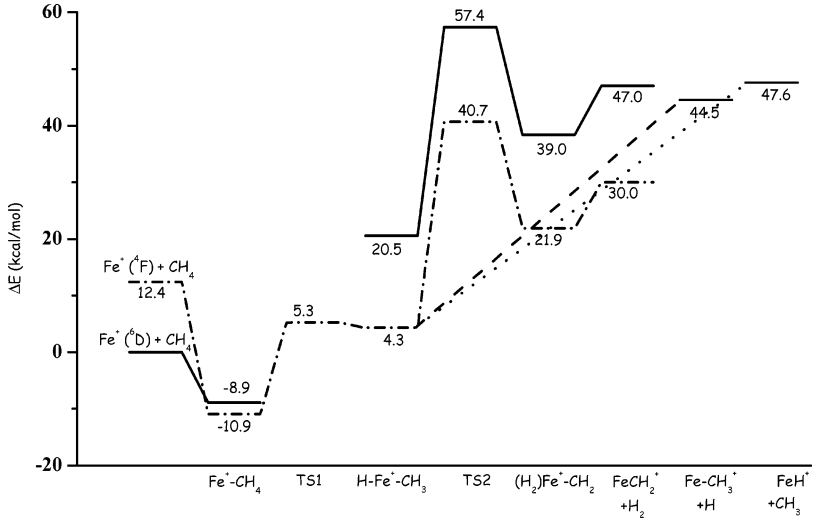

Figure 1. B3LYP/DZVP$_{opt}$ potential energy surfaces for the reaction of sextet and quartet states of Fe^+ with CH_4. Energies are in kcal/mol and relative to the ground-state reactants.

Also dehydrogenation is a process occurring at fairly low energies:

$$Fe_2^+ + CH_4 \rightarrow Fe_2CH_2^+ + H_2$$

Unlike the monomer, the formation of $Fe_2^+-CH_3$

$$Fe_2^+ + CH_4 \rightarrow Fe_2CH_3^+ + H$$

is not experimentally observed. We investigated the paths corresponding to the three multiplicities mentioned above: decaplet, octet and sextet, and the BPW91/DZVP$_{opt}$ and B3LYP/DZVP$_{opt}$ calculated potential energy surfaces are sketched in Figures 2 and 3, respectively. Corresponding geometrical parameters of octet stationary points are reported in Figure 4. Decaplet structures are always higher in energy and are not taken into account in drawing PESs. This means that if the decaplet is assumed to be the ground state of the dimer at B3LYP level, the octet excited state is much more reactive for formation of products.

At a first sight, from the sketch of the PESs reported in Figures 2 and 3, it appears that the key steps of the process are the same along the B3LYP/DZVP$_{opt}$ and BPW91/DZVP$_{opt}$ paths even if some differences exist. In analogy with the mechanism of the activation reaction of methane by the monomer, again the reaction of Fe_2^+ involves oxidative addition to form the $H-Fe_2^+-CH_3$ intermediate. To accomplish this, the first step of the reaction is the exothermic formation of the ion molecule complex $Fe_2^+(CH_4)$. From an accurate scan of all the possible approaching ways of methane to the dimer, it was concluded that the most stable complex, along the octet PES at both the hybrid B3LYP and nonhybrid BPW91 levels of theory, has a tridentate structure with the practically undistorted methane molecule interacting with only one iron atom. The two considered levels of theory, on the contrary, predict different arrangements for the sextet, that is a tridentate structure for BPW91 and a bidentate one for the B3LYP functional. Along the calculated B3LYP path the ion−molecule is stabilized by 9.4 kcal/mol with respect to the decaplet asymptote, whereas the sextet formation is only endothermic by 5.7 kcal/mol. As in going from the reactants' asymptote to the first ion−molecule intermediate, the spin multiplicity changes from decaplet to octet. In this region of the computed B3LYP PES, the unique spin crossing occurs, and the spin is conserved during the following steps. At the BPW91 level the octet complex is stabilized by 10.1 kcal/mol with respect to the octet asymptote, whereas the sextet lies 12.1 kcal/mol above the reactants' dissociation limit. The next step of the reaction is the insertion of the dimer into the C−H bond through a transition state TS1 corresponding to a hydrogen shift from carbon to iron. The structures of the first order saddle point at both the considered levels of the theory and for both octet and sextet multiplicities are very similar, and the normal mode associated with the imaginary frequency corresponds to the correct motion, namely C−H stretch and simultaneous rotation of the CH_3 group around the iron atom. Indeed, in the geometrical arrangement adopted by the insertion intermediate, $H-Fe_2^+-CH_3$(2), both the hydrogen atom and the methyl group occupy bridged positions between the iron atoms and lie in opposite planes. The B3LYP octet TS1 is characterized by an imaginary frequency of 156i cm^{-1} and a barrier height of 5.1 kcal/mol above the dissociation limit of the reactants. The barrier height is 10.9 kcal/mol at BPW91, and the value of the imaginary frequency is 669i cm^{-1}. The stabilization energy of the ground-state $H-Fe_2^+-CH_3$(2) intermediate, measured from the reactants' ground state, is 13.2 and 13.8 kcal/mol at the BPW91 and B3LYP levels, respectively. The next step, along the path that leads to molecular hydrogen elimination, consists of another hydrogen transfer from the methyl group to obtain the next intermediate and the driving force for this hydrogen transfer appears to be just the formation of molecular hydrogen by a five-centered transition state. In this region of the calculated PESs the B3LYP and BPW91 results differ to a certain extent. Indeed, at the B3LYP level the intermediate $H_2-Fe_2^+-CH_2$, which represents the direct precursor to molecular hydrogen elimination, is more stable in an octet state and its formation is exothermic by 5.2 kcal/mol. The calculated imaginary frequency for the corresponding transition state, more stable in an octet spin state, is 1417i cm^{-1} and is mainly associated with the displacement of the hydrogen atom from the carbon that is changing its hybridation. The calculated barrier height associated with this process is 22.8 kcal/mol in excess of the endothermicity of products formation and is well comparable to that experimentally estimated (25.4 ± 5.3 kcal/mol). Along the BPW91 path the five-centered transition state for the second hydrogen shift is more stable in the low spin sextet state and also the $H_2-Fe_2^+-CH_2$ intermediate has a sextet ground state. The spin is not conserved along the path and a surface crossing is likely to occur in this region

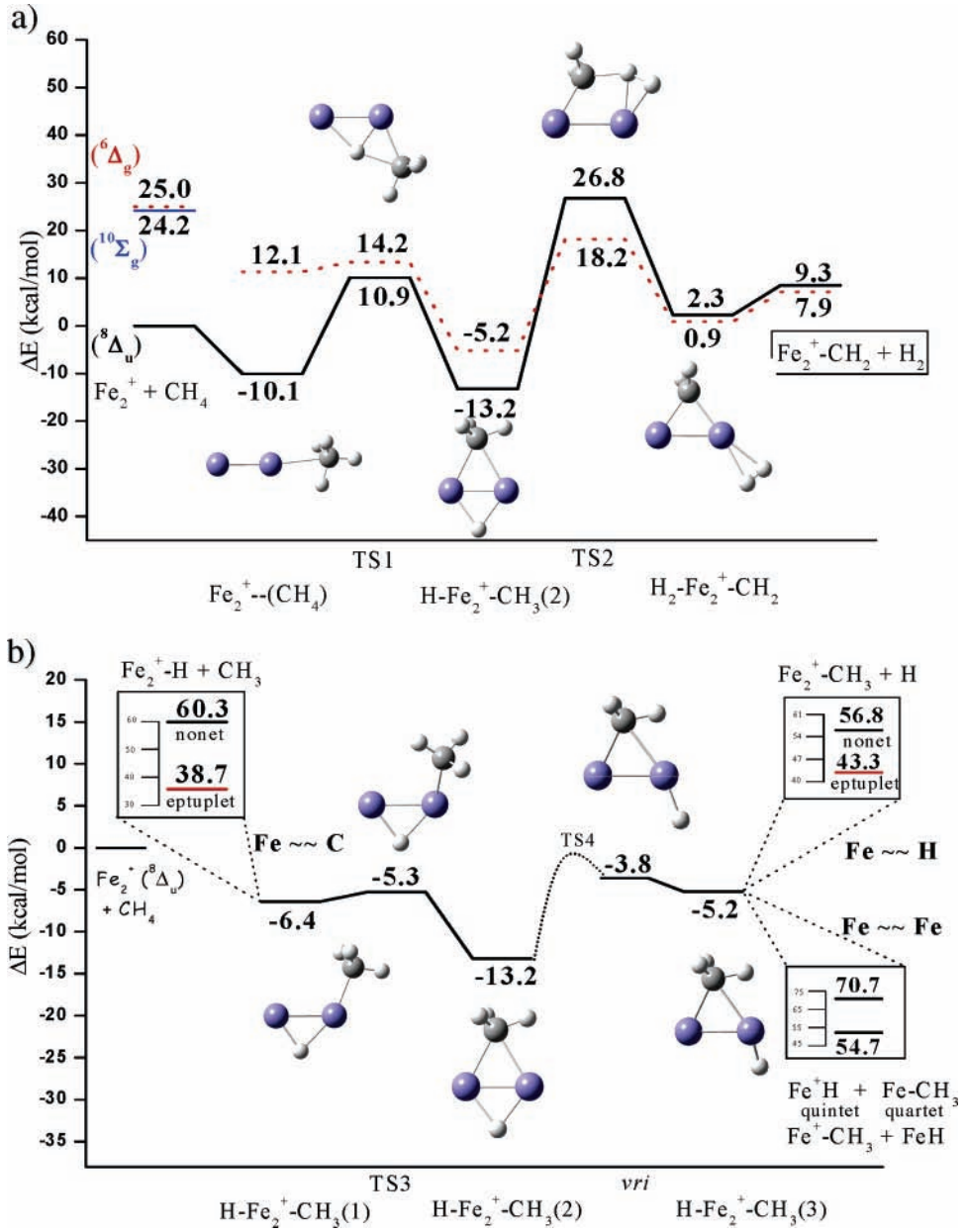

Figure 2. Potential energy surfaces for the reaction of decaplet, octet and sextet states of Fe_2^+ cation with CH_4 at the BPW91/DZVP$_{opt}$ level for (a) dihydrogen and (b) CH_3 and H eliminations. Energies are in kcal/mol and relative to the ground-state reactants.

of the PES. An imaginary frequency of 1287i cm^{-1} characterizes the corresponding sextet transition state that lies 10.3 kcal/mol above the $Fe_2CH_2^+ + H_2$ products asymptote. Although the calculated value in this case is lower than the experimentally estimated energy barrier, this step of the reaction is hampered by the spin crossing between surfaces of different multiplicities. As can be realized from geometrical parameters in Figure 4, at both hybrid and nonhybrid levels, the hydrogen molecule is practically formed at this point and an electrostatic interaction holds together the molecule and the $Fe_2CH_2^+$ ion. At the BPW91 level the sextet state of this intermediate is only slightly more stable, by 1.4 kcal/mol, than the corresponding octet one. From the $H_2-Fe_2^+-CH_2$ intermediate the reaction proceeds to yield H_2 loss in a barrierless way with the dehydrogenation products situated 0.5 and 7.9 kcal/mol above the reactants' asymptote at the B3LYP and BPW91 levels, respectively.

On the basis of the observed competition between the $Fe_2^+-CH_2$ and Fe_2^+-H products channels, it was hypothesized[28] that these products share a common intermediate. Our results agree only partially with this hypothesis as the elimination of the CH_3 group does not occur directly from the $H-Fe_2^+-CH_3$ intermediate. Further formation is required of a less stable $H-Fe_2^+-CH_3(1)$ isomer characterized by the methyl group that occupies a terminal position. This complex is obtained by surmounting an energy barrier that corresponds to the transition state, TS3, for the displacement of the methyl group from a bridged to a terminal position. Along the B3LYP PES, the $H-Fe_2^+-CH_3$-(1) isomer, which is less stable by only 6.0 kcal/mol than the global $H-Fe_2^+-CH_3$ minimum, is obtained, overcoming an energy barrier situated 3.8 kcal/mol below the reactants' dissociation limit. At the BPW91 level in going from the global minimum to the next $H-Fe_2^+-CH_3(1)$ isomer the energy decreases by 6.8 kcal/mol and the TS3 transition state, situated 5.3 kcal/mol below the reactants' asymptote, is formed. Once the $H-Fe_2^+-CH_3(1)$ intermediate is formed, the major ionic product at higher energies, Fe_2^+-H, can be obtained by barrierless breaking of the Fe−C bond to eliminate an intact methyl group. The process is predicted to be endothermic with respect to the entrance channel by 44.3 and 38.7 kcal/mol at the B3LYP and BPW91 levels, respectively. As a consequence,

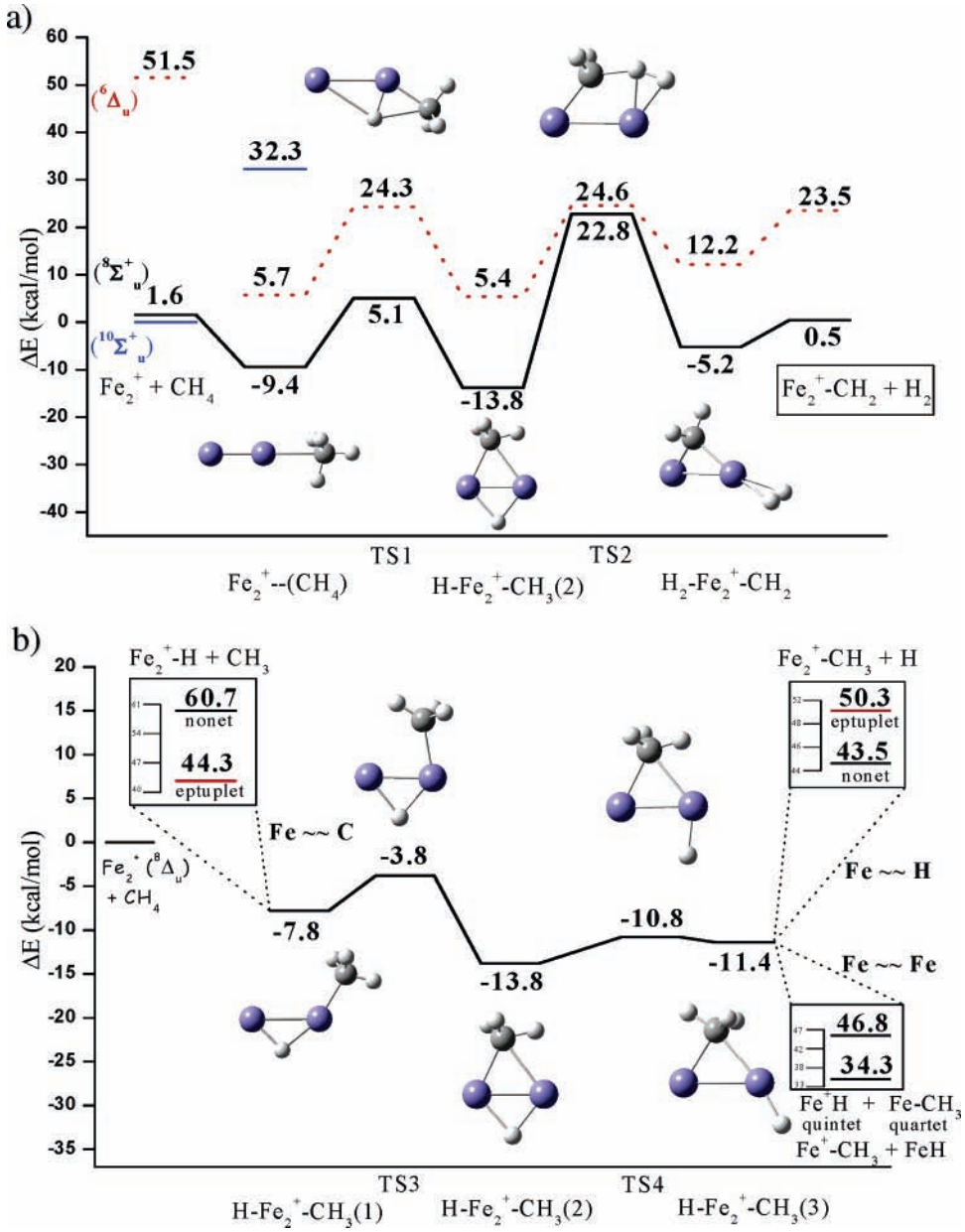

Figure 3. Potential energy surfaces for the reaction of decaplet, octet and sextet states of Fe_2^+ cation with CH_4 at the B3LYP/$DZVP_{opt}$ level for (a) dihydrogen and (b) CH_3 and H eliminations. Energies are in kcal/mol and relative to the ground-state reactants.

with respect to the situation described for the monomer, the hydride channel appears to be not dominant because also in this case the thermodynamically favored dehydrogenation reaction requires a rearrangement over a tight transition state, but the corresponding calculated barrier height is significantly lower.

As previously outlined, formation of the $Fe_2^+-CH_3$ product is not experimentally observed,[28] likely due to lack of enough experimental sensitivity combined with angular momentum conservation considerations. Here are reported the results concerning the numerous attempts that we have performed to find a possible explanation of this behavior. Analogously to what happens for the elimination of the methyl fragment, detachment of a hydrogen atom does not occur by a simple breaking of the Fe−H bond in the $H-Fe_2^+-CH_3$(2) intermediate in which the hydrogen atom occupies a bridged position. The reaction, indeed, involves formation of another hydrido−methyl $H-Fe_2^+-CH_3$-(3) complex, whose structure is characterized by the methyl group in a bridged position and the hydrogen atom in a terminal one. This last intermediate is less stable than the $H-Fe_2^+-CH_3$(2) global minimum by about 8 kcal/mol at the BPW91/$DZVP_{opt}$ level, whereas an energy difference of only 2.4 kcal/mol separates the two isomers at the B3LYP/$DZVP_{opt}$ level. Again, the BPW91 and B3LYP results differe in describing this region of the PES. To obtain the $H-Fe_2^+-CH_3$(3) intermediate along the B3LYP path, it is necessary to overcome a very low energy barrier, corresponding to the transition state for the displacement of the hydrogen atom from the bridged to the terminal position, situated 10.8 kcal/mol below the dissociation limit. Therefore, these results suggest that no mechanistic reason hampers the formation of an $Fe_2CH_3^+$ product. At the BPW91 level the fact that in the $H-Fe_2^+-CH_3$(3) complex the hydrogen occupies an out-of-plane position has important consequences (see Figure 4). Along the octet surface the C_s symmetry of the transition state is not preserved in the intermediate $H-Fe_2^+-CH_3$(3), which has C_1 symmetry. Because the IRC cannot lose a spatial symmetry while descending from a transition state toward minima along the PES, a *valley-ridge inflection point* (VRI)[76] exists on the C_s-conserved IRC. The TS4 transition state and the minimum $H-Fe_2^+-CH_3$(3), therefore, are not directly

connected, and the terminus of the IRC is another first-order saddle point (indicated in Figure 2 as *vri* and lying 3.8 kcal/mol below the reactants' dissociation limit) that connects two minima that are each other's mirror images with lower symmetry. Direct coupling of two transition states related to the bifurcation of trajectories has been widely observed,[78] and the present system provides a further example of such a behavior, which is more common than is generally appreciated. Unfortunately, any attempt to locate the octet TS4 transition states was unsuccessful, despite the numerous strategies employed, and for this reason, it is not possible to exactly establish whether it lies above or below the reactants' dissociation limit. From the outlined situation it appears that at BPW91 the elimination of a hydrogen atom is more inhibited with respect to the elimination of a methyl group, even if the obtained energetic profile does not determine that the $Fe_2CH_3^+$ product is not formed at all.

Finally, from the $H-Fe_2^+$-CH_3(3) intermediate the $Fe_2CH_3^+ + H$ products formation takes place through barrierless cleavage of the metal−hydrogen bond. The reaction products are situated at about 43 kcal/mol, at both levels, above the entrance channel and their formation is endothermic as the elimination of the methyl fragment. It is worth noting that if in the $H-Fe_2^+-CH_3$(3) intermediate a possible break of the Fe−Fe bond is accounted for, at B3LYP level formation of $Fe-CH_3$ and Fe^+-H products becomes competitive, as shown in Figure 3, with respect to a hydrogen atom elimination (34.3 kcal/mol vs 43.5 kcal/mol).

As observed in other situations,[30] the behavior of the dimer parallels to some extent that of the monomer along the paths for the reactions leading to molecular hydrogen and CH_3 and H fragments elimination. No matter the employed level of theory, the activation process involves the exothermic formation at the entrance channel of an ion−molecule complex followed by the first shift of a hydrogen atom from carbon to iron. This step is associated with a transition state characterized by an energy barrier that exceeds the energy of the reactants' dissociation limit. A second hydrogen shift through a tight transition state, lying above the energy of the entrance channel, leads to the formation of dehydrogenation products. The main difference between the PESs for the dimer with respect to those of the monomer is the stabilization of dehydrogenation products, of the intermediates and transition states localized along the PESs. This means that in contrast to the monomer the intermediates and products are thermodynamically accessible with respect to the ground-state reactants. This is the result of the stability of bridging structures where both metals are bound to a methane fragment. Moreover, the increased stability of bridged structures of intermediates acts in such a way that eliminations of the CH_3 group and H atom do not occur directly by bond breaking of the intermediate that is shared also with the dehydrogenation process. It has been suggested[29] that such bridging interactions might increase the reactivity of transition metal dimers relative to that of monomers by lowering transition-state energies. The present results for Fe_2^+ show that indeed the transition state for the rate-determining step of the dehydrogenation reaction is significantly stabilized with respect to the analogous one for the reaction of the monomer due to the involvement of both iron atoms.

Bond Energies and ELF Analysis of the Bond. Values provided by Armentrout et al. represent the first experimental thermodynamic information on the bond energies for iron dimer cation bound to H, C, CH, CH_2 and CH_3 species.[28] To the best of our knowledge no previous high level theoretical work concerning bond strength and geometrical structure of such cations exists in the literature that can help to rationalize trends in binding energy as a function of the structure. Values obtained by us at B3LYP/$DZVP_{opt}$ and BPW91/$DZVP_{opt}$ levels of theory for ligands in both bridged and terminal positions are collected in Table 3 along with corresponding experimental measurements. Geometrical parameters for the same species are reported in Figure 5.

TABLE 3: B3LYP/$DZVP_{opt}$ and BPW91/$DZVP_{opt}$ Binding Energies Corrected for BSSE (Reported in Parentheses), Calculated with Respect to the Decaplet and Octet, Respectively, Ground States of the Iron Dimer Cation, for the $Fe_2CH_3^+$, $Fe_2CH_2^+$, Fe_2CH^+, Fe_2C^+ and Fe_2H^+ Complexes with Ligands in Bridged and Terminal Positions

species	B3LYP/$DZVP_{opt}$	BPW91	exp[b]
$Fe_2CH_3^+$ (^{7}A) bridged	42.1 (3.5)	48.2 (9.1)	43.6 ± 3.7
$Fe_2CH_3^+$ (^{9}A) terminal	48.9 (3.5)	41.0 (2.8)	
$Fe_2CH_2^+$ (^{8}A) bridged	100.0 (3.6)	93.1 (5.1)	
$Fe_2CH_2^+$ (^{8}A) terminal	83.1 (3.0)	56.2 (2.8) (A″) 93.5 (6.2) (bridged ^{6}A)	78.2 ± 4.2
Fe_2CH^+ (^{7}A) bridged	110.3 (4.3)	114.9 (5.4)	70.1 ± 3.0
Fe_2CH^+ (^{7}A″) terminal	83.1 (3.9)	78.2 (4.3) (A′)	*(76.6 ± 4.6)*
Fe_2C^+ (^{8}A′) bridged	97.7 (7.6)	115.0 (4.9)	95.2 ± 6.9
Fe_2C^+ (^{8}A′) terminal	61.3 (3.2)	47.1 (4.6) (A″) 118.0 (5.9) (bridged ^{6}A′)	*(91.5 ± 8.3)*
Fe_2H^+ (^{7}A″) bridged	49.2 (2.4)	56.8 (1.2)	35.3 ± 4.6
Fe_2H^+ (^{9}A″) terminal	34.1 (1.0)	39.0 (1.3)	

[a] Experimental values are also reported for comparison. All the values are in kcal/mol. [b] Reference 28.

For each of the considered species both the possible bridging and terminal bindings have been considered and, as can be inferred from data in Table 3, in almost all cases the bridged position for the ligands is the most stable one, except for the CH_3 ligand that prefers, at the B3LYP level, a terminal position. The enhancement of stabilization of the bridged geometrical arrangement, due to the presence of two metal atoms that can form bonds toward the fragments, changes the trends of the binding energies that can be expected on the basis of the number of bonds that can be formed by the ligand in a terminal position. Binding energies, corrected for BSSE, calculated by us for the most stable structures are in all cases higher than the experimentally reported values. It is worth noting that at the B3LYP level the agreement is excellent for the bridged (^{7}A) $Fe_2CH_3^+$ and the terminal (^{9}A″) Fe_2H^+ fragments and fairly good for the terminal (^{8}A) $Fe_2CH_2^+$ fragment, which, however, in all cases do not coincide with the most stable structures. The use of the B3LYP/$DZVP_{opt}$ protocol leads to binding energy for the bridged methylene cluster cation comparable to that for the bridged diatomic iron carbide, and the CH fragment appears to be the most strongly bonded to the dimer cation. In agreement with experimental observations the bond energy of the $Fe_2CH_2^+$ fragment exceeds that of Fe_2H^+ of an amount comparable to a π metal−carbon bond (about 40 kcal/mol) for the terminal and bridged structures, although the difference is larger when the bridged species are considered. In the same way, the bond energies calculated for the most stable structures of the FeH^+ and $FeCH_2^+$ fragments, as expected, are comparable. As far as the BPW91/$DZVP_{opt}$ protocol is concerned, the obtained trend gives the C and CH fragments as the most strongly bound to the dimer cation, 118.0 and 114.9 kcal/mol, respectively, being the bond energies for the most stable bridged species. Also in this case the bond trends follow the expected behavior and in one case, that is for the bridged structure of the $FeCH_3^+$ fragment, which correspond to the most stable structure, there

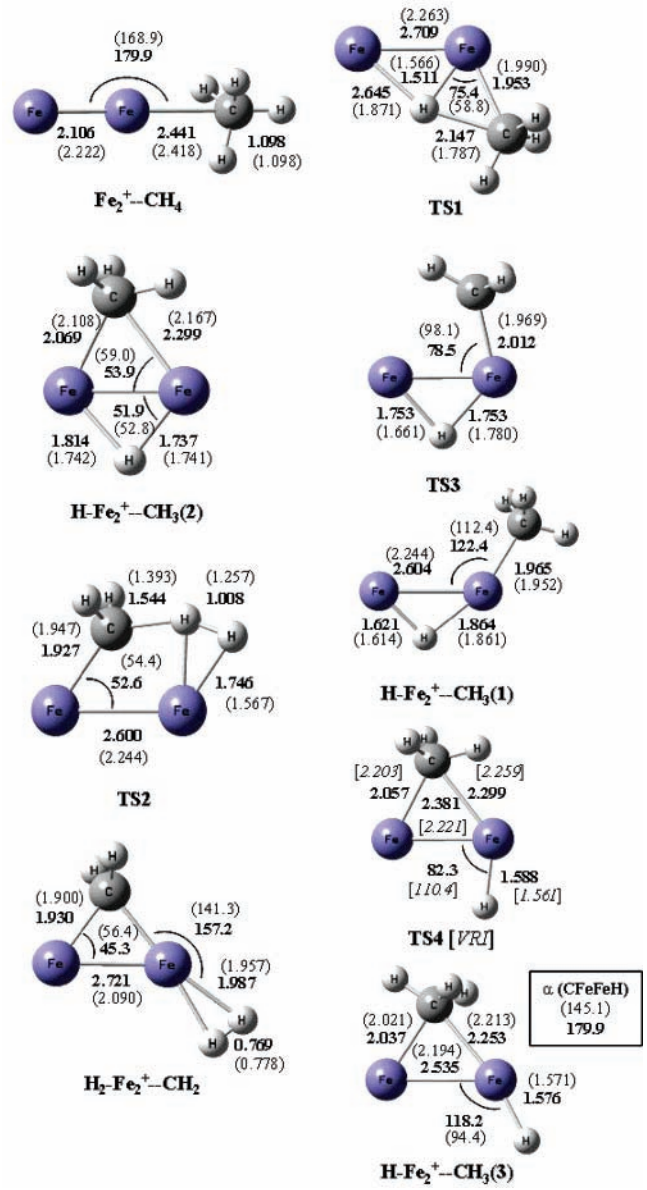

Figure 4. Geometrical parameters of the most stable B3LYP/DZVP$_{opt}$ (in bold) and BPW91/DZVP$_{opt}$ (in brackets) structures of intermediates and transition states involved in the methane activation by Fe_2^+ to yield molecular hydrogen, CH_3 and H elimination. Bond lengths are in angstroms and angles in degrees.

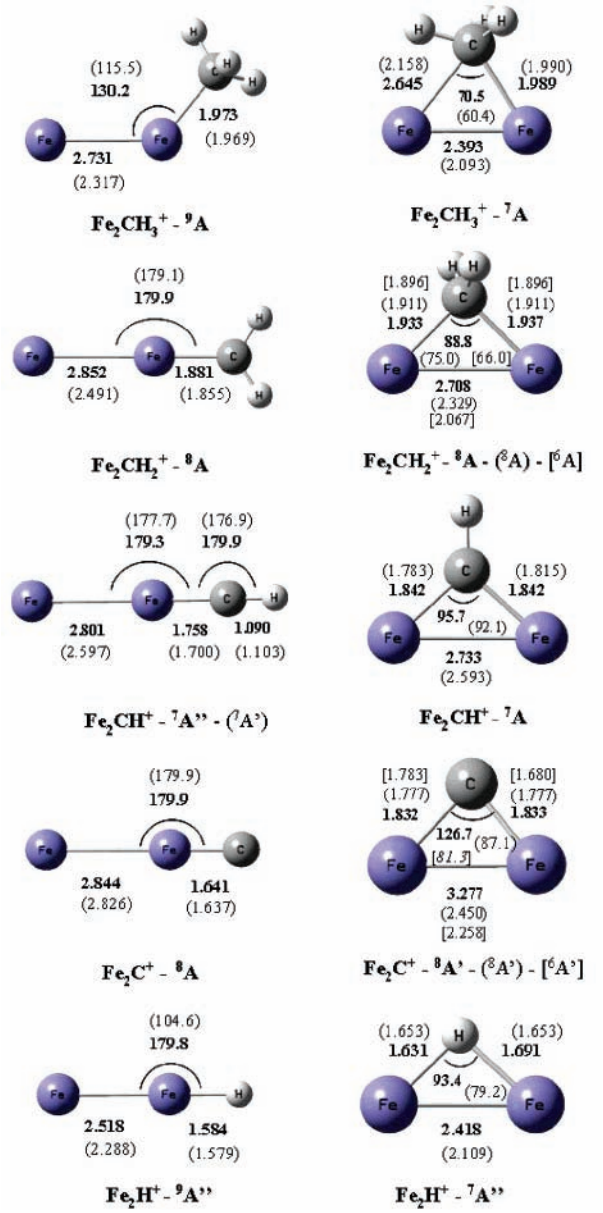

Figure 5. Geometrical parameters of B3LYP/DZVP$_{opt}$ (in bold) and BPW91/DZVP$_{opt}$ (in brackets) bridged and terminal complexes $Fe_2CH_3^+$, $Fe_2CH_2^+$, Fe_2CH^+, Fe_2C^+ and Fe_2H^+. For each structure is reported the label for the electronic state. Additional parameters are reported in square brackets when there is not coincidence between the ground states of the structure at the considered levels of theory. Bond lengths are in angstroms and angles in degrees.

is a good agreement between the calculated and measured values, considering the range of the experimental error.

We have also analyzed the characteristics of the bonding of the different product fragments at both the BPW91 and B3LYP level by using the topological analysis of the ELF function. Our BPW91 results indicate that in all cases the bridged structures are the most stable conformers. Therefore, the bonding corresponding to these structures for each fragment is described and in Figure 6 are shown the electron localization domains corresponding to all the examined fragments for the lowest-energy spin-state species. The lowest binding energies are those of the $Fe_2CH_3^+$ (48.2 kcal/mol) and Fe_2H^+ (56.8 kcal/mol) fragments. The analysis of the ELF function indicates that both structures are characterized by the presence of a trisynaptic valence basin, $V(C,Fe_1,Fe_2)$ and $V(H,Fe_1,Fe_2)$, respectively, with a similar electron population, i.e., 1.55 in the case of $Fe_2CH_3^+$ and 1.84 for Fe_2H^+. This indicates that, in both cases, the bonding between the Fe atoms and C (or H) could be considered as a three-center−two-electron bond, even when the electron population is slightly depleted (lower that 2 electrons). The presence of a disynaptic $V(Fe_1,Fe_2)$ basin with a population of 2.39 e for $Fe_2CH_3^+$ and 2.18 e for Fe_2H^+, indicates that the Fe−Fe bond can be described as a single covalent bond.

The next fragment, as increasing values of binding energies are considered, is $Fe_2CH_2^+$, which shows an important increase of the binding energy, namely, 93.5 kcal/mol (^{6}A) at the BPW91 level. The characteristics of the bonding are quite different from those for the previously described structures. Indeed, in this case the structure is characterized by the presence of two single Fe−C bonds, as indicated by the presence of two disynaptic valence basins, $V(Fe_1,C)$ with an electron population of 1.38 e and $V(Fe_2,C)$ with 1.49 e. In addition, the presence of a $V(Fe_1,Fe_2)$ disynaptic valence basin with a population of 2.36 e, indicates the presence of a single Fe−Fe covalent bond. The ^{8}A structure, which has a very close binding energy (93.1 kcal/mol), presents

similar disynaptic Fe−C basins. The main difference with respect to the $Fe_2CH_2^+$ ^6A fragment, is the lowering of the $V(Fe_1,Fe_2)$ electron population (1.75 e). The decrease of the $V(Fe_1,Fe_2)$ population with respect to the previous structures can be understood by considering the lengthening of the Fe−Fe bond distance (2.093 and 2.109 for $Fe_2CH_3^+$ and Fe_2H^+, respectively; and 2.329 for $Fe_2CH_2^+$). The ^6A state instead has an Fe−Fe bond of 2.067 Å, parallel with its higher $V(Fe_1,Fe_2)$ basin population. The presence of two Fe−C covalent bonds seems to justify the increase of the binding energies in going from $Fe_2CH_3^+$ and Fe_2H^+ to $Fe_2CH_2^+$. It should be noted that all disynaptic basins have an electron occupation lower than 2 electrons.

The next structure corresponds to the Fe_2C^+ fragment with a binding energy of 118.0 kcal/mol ($^6A'$), followed by the $^8A'$ structure with 115.0 kcal/mol. These fragments are characterized by the presence of a disynaptic $V(Fe_1,Fe_2)$ valence basin with a population lower than the previous structure, i.e., 1.51 e. In contrast, the population of the Fe−C valence basins is notably increased, i.e., $V(Fe_1,C) = V(Fe_2,C) = 2.74$ e. This indicates a strengthening of the Fe−C covalent bonds. This fact could justify the increasing of the binding energies in going from the $Fe_2CH_2^+$ to the Fe_2C^+ fragment.

Finally, the Fe_2CH^+ system has a binding energy very close to that corresponding to the Fe_2C^+ fragment according to our BPW91 calculations. The topological analysis indicates that, compared with the Fe_2C^+ fragment case, the presence of an H atom bonded to the C atom provokes an important redistribution of charge between the disynaptic basins. Indeed, the formation of a C−H bond ($V(C,H = 2.10$ e), has the effect of lowering the population of the Fe−C valence basins, i.e., $V(Fe_1,C) = 2.02$, $V(Fe_2,C) = 2.24$, mainly due to a lower electronic contribution of the C atom to that basin. On the other hand, there is an important strengthening of the Fe−Fe bond, as shown by the increasing occupation in the $V(Fe_1,Fe_2)$ disynaptic basin, which now has an occupation of 2.30 electrons, indicating a redistribution of charge density in agreement with binding energy trends.

An analogous ELF analysis carried out at the B3LYP level on the same fragments, not reported here, gives results that are coherent with the calculated binding energies trend. Populations of valence $V(Fe-C)$ basins follow the expected behavior illustrated for the analysis at the BPW91 level. The main difference concerns the population of the valence $V(Fe-Fe)$ disynaptic basins that are found very low in each case. These low populations can also be understood when the topological analysis of the electron localization function is interpreted in terms of superposition of Lewis-like mesomeric structures.[79] Indeed, as can be realized from Figure 6, B3LYP geometrical structures of fragments are characterized by longer Fe−Fe bond lengths that correspond to lower electron populations of the $V(Fe-Fe)$ basins.

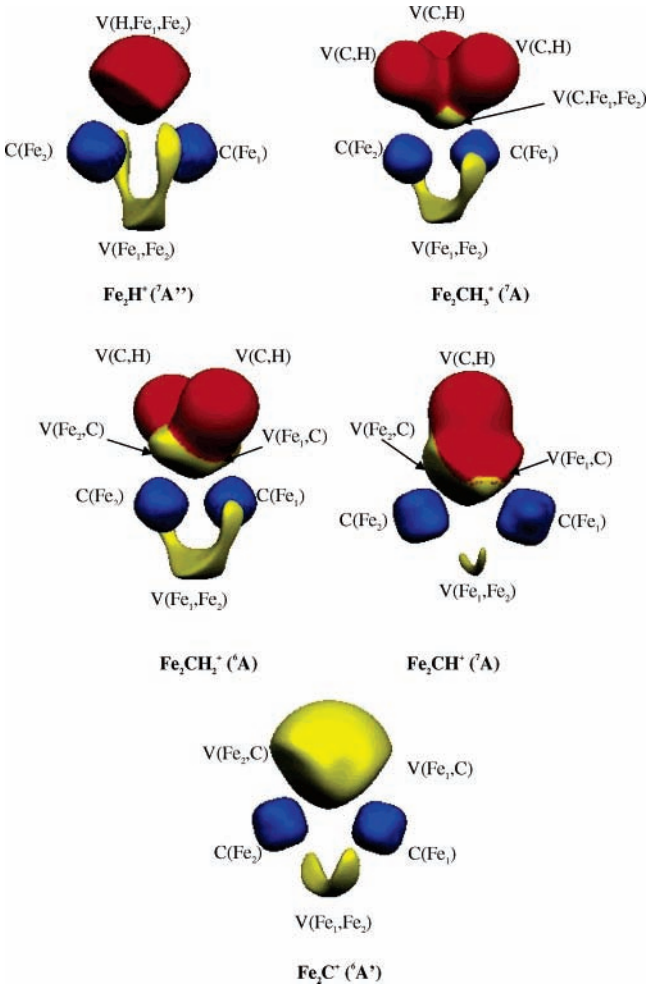

Figure 6. ELF localization domains ($\eta = 0.5$) for all the Fe_2H^+, $Fe_2CH_3^+$, $Fe_2CH_2^+$, Fe_2CH^+ and Fe_2C^+ complexes corresponding to their lowest spin multiplicities. Core basins are represented in blue, protonated disynaptic and trisynaptic basins in red, and valence disynaptic in yellow.

Conclusions

The reactivity of iron cluster cations with methane has been studied for the particular case of the dimer. To fix the energy of the reactants' asymptote, the electronic structure of the dimer has been revised in light of the use of a newly optimized basis set of double-ζ quality for iron. Minima and transition states along the PESs for three different reaction channels have been localized for the decaplet, octet and sextet multiplicities of the cation at B3LYP and BPW91 levels of theory. The detailed investigation carried out by us using both hybrid and nonhybrid approaches does not allow a complete rationalization of the experimental findings. The overall picture that can be drawn by employing the pure BPW91 functional, which has been suggested to be more appropriate in treating iron clusters, does not differ significantly with respect to that at the B3LYP level. Compared to the monomer, whose behavior has been briefly summarized, at both the considered levels of theory, the dimer ion shows a similar shape of the examined PESs but a stabilization enhancement of almost all the stationary points localized along the examined reaction paths. The preference for the bridged geometrical arrangements, due to the presence of two metal atoms that can form bonds toward the fragments, is observed along both B3LYP/$DZVP_{opt}$ and BPW91/$DZVP_{opt}$ reaction paths and the main difference concerns the assignment of the ground state for the reactants' asymptote and the region of the PESs where possible crossings between different multiplicities can occur. Stability enhancement of bridging structures is responsible also for the formation, by surpassing low energy barriers, of additional intermediates from which elimination of a H atom and a CH_3 group can occur. Molecular hydrogen loss is thermodynamically favored with respect to elimination of a methyl fragment. In comparison with the previously examined behavior of the monomer the energy barrier that must be surmounted to yield dehydrogenation products is by about 20 kcal/mol lower and the overall process appears to be significantly less endothermic. Some differences are found between the B3LYP and BPW91 descriptions of the step that leads to

the elimination of a hydrogen atom, not experimentally observed. However, no mechanistic detail supports the hypothesis that this fragment is not formed at all. Bond energies of the iron dimer cation with H and CH_x ($x = 0-3$) ligands have been calculated and compared with experimentally recommended values. Both hybrid and nonhybrid approaches give values overestimated with respect to experimentally measured values. Although trends of bond energies follow the expected behavior on the basis of simple bond order considerations the ligand's preference for the bridged position with respect to the terminal one adds further stabilization effects in agreement with the calculated values. The ELF analysis of the bond confirms this picture, showing, for example, formation of a three-center−two-electron bond for the bridged structures of Fe_2H^+ and $Fe_2CH_3^+$ fragments. Further studies, both experimental and theoretical, will serve to better understand the details of the reactivity of the dimer iron cation with methane, a system that is prototypical for the description of the interaction of methane with larger iron clusters and ultimately surfaces.

Acknowledgment. This research was funded by Università della Calabria.

References and Notes

(1) Allison, J.; Freas, R. B.; Ridge, D. P. *J. Am. Chem. Soc.* **1979**, *101*, 1332.

(2) *Gas-Phase Inorganic Chemistry*; Russel, D. H., Ed.; Plenum: New York, 1989; p 412.

(3) Armentrout, P. B.; Beauchamp, J. L. *Acc. Chem. Res.* **1993**, *26*, 213.

(4) Armentrout, P. B. In *Selective Hydrocarbons Activation*: *Principles and Progress*; Davies, J. A., Watson, P. L., Greenberg, A., Liebman, J. F., Eds.; VCH: New York, 1990.

(5) Armentrout, P. B. *Annu. Rev. Phys. Chem.* **1990**, *41*, 313.

(6) Eller, K.; Schwarz, H. *Chem. Rev.* **1991**, *91*, 1121.

(7) (a) Weisshaar, J. C. *Adv. Chem. Phys.* **1992**, *82*, 213. (b) Weisshaar, J. C. *Acc. Chem. Res.* **1993**, *26*, 213.

(8) Armentrout, P. B.; Kickel, B. L. in *Organometallic Ion Chemistry*; Freiser, B. S., Ed.; Kluwer: Dordrecht, The Netherlands, 1996.

(9) Armentrout, P. B. In *Topics in Organometallic Chemistry*; Brown, J. M., Hofmann, P., Eds.; Springer-Verlag: Berlin, 1999.

(10) Crabtree, R. H. *The Organometallic Chemistry of the Transition Metals*, 2nd ed.; John Wiley & Sons: New York, 1994.

(11) Somorjai, G. A. *Introduction to Surface Chemistry and Catalysis*; John Wiley & Sons: New York, 1994.

(12) Musaev, D. G.; Morokuma, K. *J. Chem. Phys.* **1994**, *101*, 10697.

(13) Irigoras, A.; Fowler, J. E.; Ugalde, J. M. *J. Phys. Chem.* **1998**, *102*, 293.

(14) Irigoras, A.; Fowler, J. E.; Ugalde, J. M. *J. Am. Chem. Soc.* **1999**, *121*, 574; *ibid*. Irigoras, A.; Fowler, J. E.; Ugalde, J. M. *J. Am. Chem. Soc.* **1999**, *121*, 8549.

(15) Irigoras, A.; Elizalde, O.; Silanes, I.; Fowler, J. E.; Ugalde, J. M. *J. Am. Chem. Soc.* **2000**, *122*, 114.

(16) Abashkin, Y. G.; Burt, S. K.; Russo, N. *J. Phys. Chem.* **1997**, *101*, 8085.

(17) Russo, N.; Sicilia, E. *J. Am. Chem. Soc.* **2001**, *123*, 2588.

(18) Russo, N.; Sicilia, E. *J. Am. Chem. Soc.* **2002**, *124*, 1471.

(19) Michelini, M. C.; Russo, N.; Sicilia, E. *J. Phys. Chem.* **2002**, *106*, 8937.

(20) Michelini, M. C.; Russo, N.; Sicilia, E. *Inorg. Chem.* **2004**, *43*, 4944.

(21) Chiodo, S.; Kondakova, O.; Irigoras, A.; Michelini, M. C.; Russo, N.; Sicilia, E.; Ugalde, J. M. *J. Phys. Chem.* A **2004**, *108*, 1069.

(22) Jiang; L.; Xu, Q. *J. Am. Chem. Soc.* **2005**, *127*, 42.

(23) Trevor, D. J.; Cox, D. M.; Kaldor, A. *J. Am. Chem. Soc.* **1990**, *112*, 3742.

(24) Fayet, P.; Kaldor, A.; Cox, D. M. *J. Chem. Phys.* **1990**, *92*, 254.

(25) (a) Schnabel, P.; Irion, M. P. *Ber. Bunsen-Ges. Phys. Chem.* **1992**, *96*, 1101. (b) Irion, M. P.; Schnabel, P. *Ber. Bunsen-Ges. Phys. Chem.* **1992**, *96*, 1091. (c) Lian, L.; Su, C.-X.; Armentrout, P. B. *J. Chem. Phys.* **1992**, *97*, 4072.

(26) Guo, B. C.; Kerns, K. P.; Castleman, A. W. *J. Chem. Phys.* **1992**, *96*, 6931.

(27) (a) Jiao, C. Q.; Freiser, B. S. *J. Phys. Chem.* **1995**, *99*, 10723. (b) Berg, C.; Schindler, T.; Lammers, A.; Niedner-Schatteburg, G.; Bondybey, V. E. *J. Phys. Chem.* **1995**, *99*, 15497.

(28) Liyanage, R.; Zhang, X.-G.; Armentrout, P. B. *J. Chem. Phys.* **2001**, *115*, 9747.

(29) Koszinowski, K.; Schröder, D.; Schwarz H. *J. Phys. Chem. A* **2003**, *107*, 4999.

(30) Koszinowski, K.; Schlangen, M.; Schröder, D.; Schwarz H. *Int. J. Mass Spectrom.* **2004**, *237*, 19.

(31) Wright, P. G.; Ashmore, P. G.; Kemball, C. *Trans. Faraday Soc.* **1958**, *54*, 1692.

(32) Tatewaki, H.; Tomonari, M.; Nakamura, T. *J. Chem. Phys.* **1988**, *88*, 6419.

(33) Chen, J. L.; Wang, C. S.; Jackson, K. A.; Pederson, M. R. *Phys. Rev. B: Condens. Matter* **1991**, *44*, 6558.

(34) Cheng, H. P.; Ellis, D. E. *J. Chem. Phys.* **1991**, *94*, 3735.

(35) Castro, M.; Salahub, D. R. *Phys. Rev. B: Condens Matter* **1993**, *47*, 10955.

(36) Castro, M.; Salahub, D. R. *Phys. Rev. B: Condens Matter* **1994**, *49*, 11842.

(37) Castro M. Zacarias A. *Book of Abstracts*, 214th ACS National Meeting, Las Vegas, NV, September 7−11; American Chemical Society: Washington, DC, 1997; Vol. 213, p 374.

(38) Chrètien, S.; Salahub, D. R. *Phys. Rev. B: Condens Matter* **2002**, *66*, 155425.

(39) Ballone, P.; Jones, R. O. *Chem. Phys. Lett.* **1995**, *233*, 632.

(40) Besley, N. A.; Johnston, R. L.; Stace A. J.; Uppenbrink J. *THEOCHEM* **1995**, *341*, 75.

(41) Gong, X. G.; Zheng, Q. Q. *J. Phys.: Condens. Matter* **1995**, *7*, 2421.

(42) Bouarab, S.; Vega, A.; Alonso, J. A.; Iniguez, M. P. *Phys. Rev. B: Condens. Matter* **1996**, *54*, 3003.

(43) Bobadova-Parvanova, P.; Jackson, K. A.; Srinivas, S.; Horoi, M.; Kohler, C.; Seifert, G. *J. Chem. Phys.* **2002**, *116*, 3576.

(44) Bobadova-Parvanova, P.; Jackson, K. A.; Srinivas S.; Horoi, M. *Phys. Rev. B: Condens. Matter* **2002**, *66*, 195402/1.

(45) Postnikov, A. V.; Entel, P.; Soler, J. M. *Mater. Res. Soc. Symp. Proc.* **2002**, *704*, 225.

(46) Irigoras, A.; Michelini, M. C.; Sicilia, E.; Russo, N.; Mercero, J. M.; Ugalde, J. M. *Chem. Phys. Lett.* **2003**, *376*, 310.

(47) Gutsev, G. L.; Bauschlicher, C. W., Jr. *J. Phys. Chem. A* **2003**, *107*, 7013.

(48) Fossan, K. O.; Uggerund, E. *Dalton Trans.* **2004**, *6*, 892.

(49) Chrètien, S.; Salahub, D. R. *J. Chem. Phys.* **2003**, *119*, 12279.

(50) Chrètien, S.; Salahub, D. R. *J. Chem. Phys.* **2003**, *119*, 12291.

(51) Gutsev, G. L.; Bauschlicher, C. W., Jr.; Andrews, L. *J. Chem. Phys.* **2003**, *119*, 3681.

(52) Gutsev, G. L.; Mochena, M. D.; Bauschlicher, C. W., Jr. *Chem. Phys.* **2005**, *314*, 291.

(53) Niu, S.; Hall, M. B. *Chem. Rev.* **2000**, *100*, 353.

(54) Harrison, J. F. *Chem. Rev.* **2000**, *100*, 679.

(55) Gutsev, G. L.; Bauschlicher, C. W., Jr. *J. Phys. Chem. A* **2003**, *107*, 4755.

(56) Baker, J.; Pulay, P. *J. Comput. Chem.* **2003**, *10*, 1184.

(57) Schultz, N. E.; Zhao, Y.; Truhlar, D. G. *J. Phys. Chem. A* **2005**, *109*, 11127.

(58) Schultz, N. E.; Zhao, Y.; Truhlar, D. G *J. Phys. Chem. A* **2005**, *109*, 4388.

(59) Becke, A. D. *J. Chem. Phys.* **1993**, *98*, 5648.

(60) Stephens, P. J.; Devlin, F. J.; Chabalowski, C. F.; Frisch M. J. *J. Phys. Chem.* **1994**, *98*, 11623.

(61) Becke, A. D. *Phys. Rev. A* **1988**, *38*, 3098.

(62) Perdew, J. P.; Wang, Y. *Phys. Rev. B* **1991**, *45*, 13244.

(63) Andzelm, J.; Radzio, E.; Salahub, D. R. E. *J. Comput. Chem.* **1985**, *6*, 520.

(64) Chiodo, S.; Russo, N.; Sicilia, E. *J. Comput. Chem.* **2005**, *26*, 175.

(65) Moore, C. E. *Atomic Energy Levels*; NSRD-NBS, USA; U.S. Government Printing Office: Washington, DC, 1991; Vol 1.

(66) Goudbout, N.; Salahub, D. R.; Andzelm, J.; Wimmer, E. *Can. J. Chem.* **1992**, *70*, 560.

(67) Schwarz, H. *Int. J. Mas. Spectrom.* **2004**, *237*, 75.

(68) Boys, S. B.; Bernardi, F. *Mol. Phys.* **1970**, *19*, 553.

(69) Frisch, M. J.; Trucks, G. W.; Schlegel, H. B.; Scuseria, G. E.; Robb, M. A.; Cheesman, J. R.; Zakrzewski, V. G.; Montgomery, J. A., Jr.; Stratmann, R. E.; Burant, J. C.; Dapprich, S.; Millam, J. M.; Daniels, A. D.; Kudin, K. N.; Strain, M. C.; Farkas, O.; Tomasi, J.; Barone, V.; Cossi, M.; Cammi, R.; Mennucci, B.; Pomelli, C.; Adamo, C.; Clifford, S.; Ochterski, J.; Petersson, G. A.; Ayala, P. Y.; Cui, Q.; Morokuma, K.; Malick, D. K.; Rabuck, A. D.; Raghavachari, K.; Foresman, J. B.; Cioslowski, J.; Ortiz, J. V.; Stefanov, B. B.; Liu, G.; Liashenko, A.; Piskorz, P.; Komaromi,

I.; Gomperts, R.; Martin, R. L.; Fox, D. J.; Keith, T.; Al-Laham, M. A.; Peng, C. Y.; Nanayakkara, A.; Gonzalez, C.; Challacombe, M.; Gill, P. M. W.; Johnson, B. G.; Chen, W.; Wong, M. W.; Andres, J. L:, Head-Gordon, M.; Replogle, E. S.; Pople, J. A. *Gaussian 98*; Gaussian, Inc.: Pittsburgh, PA, 1998.

(70) Silvi, B.; Savin, A. *Nature* **1994**, *371*, 683.

(71) Becke, A. D.; Edgecombe, K. E. *J. Chem. Phys.* **1990**, *92*, 5397.

(72) Noury, S.; Krokidis, X.; Fuster, F.; Silvi, B. *TopMod Package*; Paris, 1997.

(73) Noury, S.; Krokidis, X.; Fuster, F.; Silvi, B. *Comput. Chem*. **1999**, *23*, 597.

(74) MOLEKEL 4.3 visualization package. CSCS, Swiss National Supercomputing Centre. http://www.cscs.ch/molekel/

(75) Scultz, R. H.; Elkind, J. L.; Armentrout, P. B. *J. Am. Chem. Soc*. **1988**, *110*, 411.

(76) Haynes, C. L.; Chen, Y.-M.; Armentrout, P. B. *J. Phys. Chem.* **1996**, *100*, 111.

(77) Valtazanos, P.; Elbert, S. T.; Xantheas, S.; Ruedenberg, K. *Theor. Chim. Acta* **1991**, *78*, 287. Xantheas, S.; Valtazanos, P.; Ruedenberg, K. *Theor. Chim. Acta* **1991**, *78*, 327. Xantheas, S.; Valtazanos, P.; Ruedenberg, K. *Theor. Chim. Acta* **1991**, *78*, 327. Xantheas, S.; Elbert, S. T.; Ruedenberg, K. *Theor. Chim. Acta* **1991**, *78*, 365. Valtazanos, P.; Ruedenberg, K. *Theor. Chim. Acta* **1991**, *78*, 397.

(78) See for example: Kumeda, Y.; Taketsugu, T. *J. Chem. Phys.* **2000**, *113*, 477. Taketsugu, T.; Tajima, N.; Hirao, K. *J. Chem. Phys.* **1996**, *105*, 1933. Yanai, T.; Taketsugu, T.; Hirao, K. *J. Chem. Phys.* **1997**, *107*, 1137. Bartsch, R. A.; Chae, Y. M. C.; Ham, S.; Birney, D. M. *J. Am. Chem. Soc.* **2001**, *123*, 7479. Quapp, W.; Melnikov, V. *Phys. Chem. Chem. Phys.* **2001**, *3*, 2735. Singleton, D. A.; Hang, C.; Szymanski, M. J.; Meyer, M. P.; Leach, A. G.; Kuwata, K. T.; Chen, J. S.; Greer, A.; Foote, C. S.; Houk, K. N. *J. Am. Chem. Soc.* **2003**, *125*, 1319.

(79) Pilme, J.; Silvi, B.; Alikhani, M. E. *J. Phys. Chem. A* **2003**, *107*, 4506−4514; *J. Phys. Chem. A* **2005**, *109*, 10028.